

Stable High-Efficiency CsPbI₂Br Solar Cells by Designed Passivation Using Multifunctional 2D Perovskite

Jie Xu, Jian Cui, Shaomin Yang, Zhike Liu,* Xi Guo, Yuhang Che, Dongfang Xu, Wenjing Zhao, Ningyi Yuan, Jianning Ding, and Shengzhong (Frank) Liu*

CsPbI₂Br perovskite is known for its advantages over its organic-inorganic hybrid counterpart including better thermal stability and appropriate bandgap for the front sub-cell of tandem solar cell. However, its lower-than-satisfactory efficiency, problematic phase stability and sensitivity to moisture hinder its further advancement. Here, three kinds of glycine halides (Gly-X: X = Cl, Br, and I) are strategically designed to improve the performance of CsPbI₂Br perovskite solar cells (PSCs). Systematic experimental and calculated results prove that a 2D/3D hybrid structure is formed, wherein the Gly-X-based 2D perovskite is mainly located at the CsPbI₂Br grain boundaries, and the A-sites of the 2D perovskite form strong bonds with the 3D perovskite to suppress ion migration by increasing its activation energy. As a result, a power conversion efficiency (PCE) of 17.26% was obtained with an open-circuit voltage (V_{OC}) of 1.33 V, which is among the best PCE values for the CsPbI₂Br PSCs. In addition, the efficiency of encapsulated device decrease only by 14.1% after 340 h continuous illumination in ambient conditions, representing one of the most-stable inorganic PSCs reported so far. This work provides important insights into designing passivating agents to address the issue of phase segregation for the development of highly stable perovskite optoelectronic devices.

1. Introduction

In the past ten years, organic-inorganic hybrid perovskite solar cells (PSCs) have become superstars in the field of photovoltaics, attracting extensive attention from both the scientific community and industry. However, hybrid PSCs are quite vulnerable to heat and moisture, which substantially hampers their future commercialization. In the past several years, cesium-based all-inorganic perovskites have attracted increasing attention as a result of their excellent thermal stability and quickly increasing efficiency, providing a new possibility for fabricating more-stable PSCs. As a kind of cesium-based all-inorganic perovskite material, CsPbI₂Br shows good α -phase stability at room temperature due to its lowered phase transition temperature and increased tolerance factor,^[1] exhibits excellent thermal stability even at >350 °C,^[2] and has an appropriate bandgap (1.91 eV) as the top cell for tandem solar cell

applications.^[3] However, CsPbI₂Br perovskite faces three serious problems in applications. First, CsPbI₂Br is moisture sensitive and easily transforms from black α -phase to yellow nonperovskite phase in humid conditions. Second, mixed-halide CsPbI₂Br perovskites usually suffer from serious phase segregation under light illumination. Third, CsPbI₂Br easily forms point defects, such as iodide vacancies (V_I), Pb-I antisite defects, and interstitial/undercoordinated Pb²⁺ ions, resulting in much lower PCE in comparison with their organic-inorganic hybrid counterparts.^[4] Therefore, strategies to block moisture, passivate defects and suppress ion migration are crucial for enhancing the efficiency and stability of CsPbI₂Br PSCs.


To date, it has been accepted that halide anions are the most mobile ions, and halide vacancies are the most prevalent point defects in mixed-halide perovskites due to their low formation and activation energies.^[5] Meanwhile, the halide ions migrate within grains by means of halide vacancies. Grain boundaries (GBs) possess high surface energy and a large number of defects, and they are not only the places where phase transition first occurs and paths for water vapor intrusion, but also areas with a high incidence area of ion migration. Therefore, how to passivate the defects at GBs and block the migration near GBs are very important issues that must be addressed to enhance the stability of mixed-halide perovskite. Thus, tremendous

J. Xu, J. Cui, S. Yang, Z. Liu, X. Guo, Y. Che, D. Xu, W. Zhao, S. (F.) Liu
Key Laboratory of Applied Surface and Colloid Chemistry
Ministry of Education; Shaanxi Key Laboratory for Advanced Energy
Devices

Shaanxi Engineering Lab for Advanced Energy Technology
School of Materials Science and Engineering
Shaanxi Normal University
Xi'an 710119, P. R. China
E-mail: zhike2015@snnu.edu.cn; liusz@snnu.edu.cn

N. Yuan, J. Ding
School of Materials Science and Engineering Jiangsu Collaborative
Innovation Center of Photovoltaic Science and Engineering Jiangsu
Province Cultivation Base for State Key Laboratory of Photovoltaic
Science and Technology
Changzhou University
Changzhou 213164, P. R. China

S. (F.) Liu
iChEM
Dalian Institute of Chemical Physics
University of Chinese Academy of Sciences
Dalian National Laboratory for Clean Energy
Chinese Academy of Sciences
Dalian 116023, P. R. China

 The ORCID identification number(s) for the author(s) of this article
can be found under <https://doi.org/10.1002/adfm.202202829>.

DOI: 10.1002/adfm.202202829

efforts have been made to passivate GBs or block ion migration near GBs by using organic halides, amino acids, ammonium salts, Lewis bases/acids, ionic liquids, and 2D perovskites;^[6–12] however, most additives with a passivation effect are incapable of blocking ion migration pathways. So there is still a lack of an effective method to both passivate GBs and block ion migration near GBs at the same time.

In this work, we strategically designed three kinds of glycine halides (Gly-X) as passivating agents to improve the performance of CsPbI₂Br solar cells. In the course of crystallization, Gly-X can modulate the crystallization process of perovskite to improve its quality. In the crystallized film, 2D Gly₂PbI₄ perovskite was formed at the GBs of 3D domains. As one benefit, the C=O and –OH groups in the A-site of 2D Gly₂PbI₄ perovskite can effectively passivate the surface defects at GBs and create a strong interaction with 3D perovskite to block the migration of halide ions for enhancing the photostability of CsPbI₂Br perovskite. Additionally, the 2D Gly₂PbI₄ perovskite at the GBs can effectively prevent the penetration of moisture, thereby greatly improving the phase stability of the CsPbI₂Br perovskite. The optimized PSCs with a Gly₂PbI₄/CsPbI₂Br hybrid configuration deliver a champion PCE of 17.26%, which is one of the best values reported for CsPbI₂Br PSCs. Furthermore, 96.6% or 85.9% of their initial efficiencies is retained after 50 days storage or 340 h continuous light illumination in ambient conditions, respectively. As such, our work demonstrates an effective strategy to address the issue of ion migration and paves the way for the development of high-performance mixed-halide perovskites with high photostability and phase stability.

2. Results and Discussion

Gly-X (X = Cl, Br and I) was synthesized by the reaction of hydrogen halides and glycine (Gly),^[13–15] and the chemical structures of Gly-X are presented in Figure S1 in Supporting Information. A small amount of Gly-X was added into the precursor solution with an optimized Gly-X/PbI₂ molar ratio of 6.0%. Comparative photographs of CsPbI₂Br films without or with 6% Gly-X additive after annealing at 40 °C for different times are shown in Figure 1a. According to the variation of colors, Gly-I can significantly decelerate the crystallization process of CsPbI₂Br, which may be beneficial to improving the quality of the perovskite film.^[16,17] Scanning electron microscopy (SEM) was conducted to explore the influence of Gly-X additives on the morphology of the CsPbI₂Br perovskite film (Figure S2, Supporting Information). The control CsPbI₂Br film without additive shows a porous surface with many gullies; in contrast, the films with Gly-X additive show a dense surface and the gullies were not observed. Top-view SEM images of perovskite films with different concentrations of Gly-I additive are exhibited in Figure S3 in Supporting Information. The film with the 6% Gly-I additive shows a dense surface and large grain, which is better than the other films. The cross-sectional SEM images of perovskite films are shown in Figure S4 in Supporting Information. The perovskite film with Gly-I was compact with fewer boundaries, which is beneficial for improving the charge transfer and photovoltaic efficiency.

In order to probe the effects of the Gly-X additives on the crystallinity of the perovskite, X-ray diffraction (XRD) patterns of CsPbI₂Br without and with Gly-X additives are analyzed (Figure S5a, Supporting Information). All the films show similar diffraction peaks at 14.58° and 29.48° that correspond to the (100) and (200) crystal planes of CsPbI₂Br perovskite, respectively.^[18,19] Compared with the control perovskite film, the peak intensities of the CsPbI₂Br films with Gly-X are increased, while the thicknesses of films are not changed, indicating that these Gly-X additives are conducive to film growth along the (100) orientation. Ultraviolet-visible spectroscopy (UV-vis) absorption measurements are carried out to study the effect of Gly-X additives on the optical properties of the CsPbI₂Br films (Figure S5b, Supporting Information). The absorption edges of the films with Gly-X additives are not shifted, but the absorption intensity in the 450–630 nm wavelength range is slightly increased, which could be due to enhanced crystallinity of the perovskite film. The XRD and UV-vis results indicate that a small amount of Gly-X additives can improve the crystallinity of perovskite film but don't change the crystal structure. The XRD patterns of CsPbI₂Br films with various concentrations of Gly-I additives are also analyzed (Figure S6a, Supporting Information). The peak intensities increase gradually with increasing concentration of Gly-I additive, reaching a maximum at 6% Gly-I. The absorption intensities of CsPbI₂Br perovskite films with Gly-I are enhanced slightly, which is ascribed to increased crystallinity (Figure S6b, Supporting Information).

In order to explore the effect of Gly-X additives on the recombination dynamics of the charge carriers in perovskite films, steady-state photoluminescence (SSPL) spectra and time-resolved PL (TRPL) curves were obtained under the excitation by a laser with 510 nm wavelength. (Figure S7, Supporting Information). The TRPL curves are fitted with a double-exponential function, and the fitted parameters are exhibited in Table S1 in Supporting Information. The perovskite film with Gly-I additive shows the highest PL intensity and longest PL decay lifetime. The average carrier lifetime was increased from 19.30 ns for the control film to 31.95 ns for the CsPbI₂Br film with Gly-I additive, which can be ascribed to effective passivation by Gly-I. The SSPL spectra and TRPL curves of perovskite films with different concentrations of Gly-I additive are also examined (Figure S8, Supporting Information). The CsPbI₂Br film with 6% Gly-I shows the strongest SSPL intensity and the most extended carrier lifetime, indicating that optimized Gly-I additive can effectively passivate the defects of perovskite film to prolong the carrier lifetime.

A large amount of research has found that the addition of large organic iodide often produces 2D perovskite in the 3D perovskite film.^[20–23] In order to determine the reaction between Gly-X and PbI₂, Gly-X, and PbI₂ in a molar ratio of 2:1 were dissolved in DMSO and spin-coated onto TiO₂ substrate for XRD measurement, as shown in Figure S9a in Supporting Information. A new strong diffraction peak at 8.24° appears in the film with Gly-I and PbI₂ as precursor, which is obviously different from the XRD patterns of Gly-I and PbI₂ (Figure S9b,c, Supporting Information), and is attributed to 2D Gly₂PbI₄ perovskite.^[24,25] 2D perovskite film was also confirmed by UV-vis measurements (Figure S10, Supporting Information). The absorption peak is located at ≈400 nm rather than 650 nm, which corresponds to 2D perovskite with a wide band

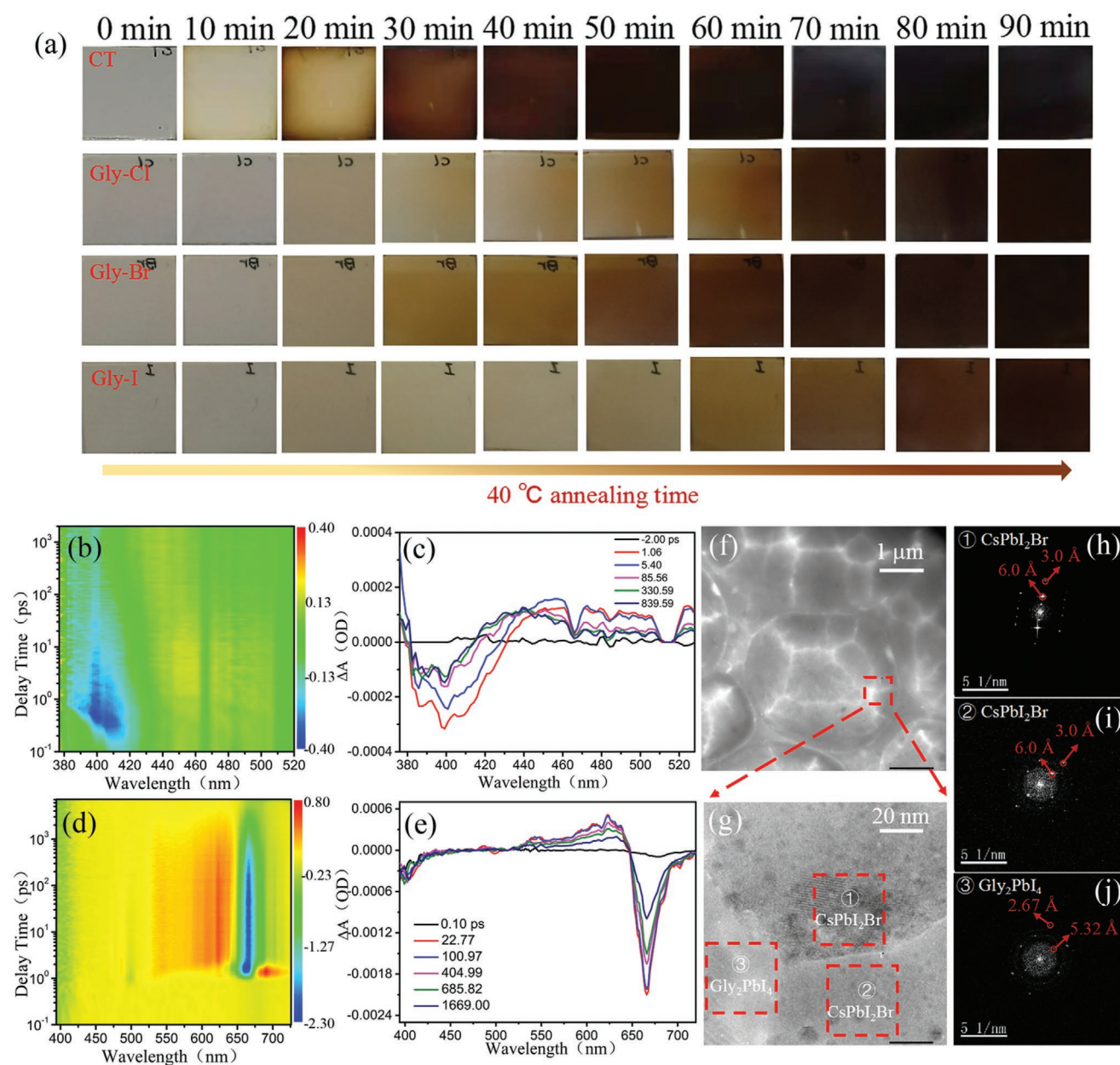


Figure 1. a) Photographs of CsPbI₂Br precursor films w/o 6% Gly-X additives after annealing at 40 °C for different times. b) Transient absorption (TA) spectrum and c) TA spectra at various delay times for the pure 2D Gly₂PbI₄ film. d) TA spectrum and e) TA spectra at various delay times for CsPbI₂Br film with Gly-I additive. f) TEM image of perovskite crystals with Gly-I additive. g) Enlarged TEM image of the area inside the red box in (f). h–j) Corresponding fast Fourier transform (FFT) analysis images.

gap (3.07 eV). Therefore, when Gly-X is used as an additive in the precursor of 3D perovskite, a small amount of 2D Gly₂PbI₄ perovskite will be formed in the film. To confirm the above deduction, perovskite precursor with 30% Gly-I additive was prepared and crystallized for XRD and UV–vis measurements (Figure S11a,b, Supporting Information). A strong diffraction peak at 8.27° corresponding to 2D Gly₂PbI₄ perovskite can be observed in the perovskite film.^[26] Meanwhile, the two absorption peaks at ≈400 and 650 nm were observed in the UV–vis spectrum and are attributed to 2D Gly₂PbI₄ and 3D CsPbI₂Br perovskite, respectively. In contrast, as shown in Figure S12a,b,

it is difficult for Gly-Br or Gly-Cl to react with PbI₂ to form 2D Gly₂PbI₂Br₂ or Gly₂PbI₂Cl₂, and the reason is not yet clear.

To further demonstrate the existence of 2D Gly₂PbI₄ in the perovskite film with 6% Gly-I additive, transient absorption (TA) measurement was conducted (Figure 1b–e). For 3D CsPbI₂Br perovskite, only one single photobleaching (PB) peak at ≈660 nm is observed (Figure S13a,b, Supporting information). For pure 2D Gly₂PbI₄ perovskite (Figure 1b,c), a dominant absorption peak is located at ≈400 nm. In contrast, for the perovskite film with 6% Gly-I added, a weak PB peak at ≈400 nm is clearly observed (Figure 1e) and attributed to 2D Gly₂PbI₄.

The TA result proves that 2D Gly₂PbI₄ perovskite is formed in the perovskite films with 6% Gly-I added. This result is consistent with the previous XRD and UV-vis results.^[27–29] To further confirm the existence of Gly₂PbI₄ in the perovskite film with 6% Gly-I added, transmission electron microscopy (TEM) was employed to examine the detailed structural information of the GBs domains in the perovskite film. Figure 1f–j exhibit the TEM, high-resolution transmission electron microscopy and corresponding fast Fourier transform (FFT) images of CsPbI₂Br film with 6% Gly-I additive. For the two perovskite grains, the FFT images are shown in Figure 1h,i, where the planes with spacings of 3 and 6 Å can be indexed to the (200) and (100) planes of CsPbI₂Br perovskite, respectively.^[30] For the region between grains, the diffraction spots obtained by FFT are shown in Figure 1j. The planes with spacings of 2.67 and 5.32 Å can be indexed to the (200) and (100) planes of 2D Gly₂PbI₄ perovskite, respectively. The TEM characterizations confirm the 2D/3D hybrid configuration is formed, wherein the 2D Gly₂PbI₄ perovskite is located at the GBs of 3D domains.^[11,12]

The Gly-X have Lewis base groups of both carbonyl (C=O) and ammonium (NH₃⁺) and different halogen anions (Cl[−], Br[−], and I[−]). To further confirm the interaction between the Gly-X and perovskite, Fourier transform infrared (FTIR) spectroscopy was performed on the pure Gly-X or PbI₂ films with the Gly-X additives. As shown in FTIR spectra (Figure 2a–c), the C=O bond of Gly-Cl exhibits a stretching vibration at 1676 cm^{−1}, which shows a downward shift to 1607 cm^{−1} after mixing with PbI₂. Similarly, the C=O signals of Gly-Br and Gly-I at 1696 and 1695 cm^{−1} shift to 1622 and 1596 cm^{−1}, respectively, after mixing with PbI₂. The downward shift of C=O in Gly-X after mixing with PbI₂ is due to electron delocalization when a Lewis base-acid adduct formed, which is evidence for the strong interaction between Gly-X and perovskite. Obviously, the C=O peak of Gly-I shows the largest downward shift from 1695 to 1596 cm^{−1}. Meanwhile, the NH₃⁺ vibrational stretch peaks in the Gly-Cl and Gly-Br are shifted from 3047 to 3098 cm^{−1} and 3036 to 3092 cm^{−1}, respectively, after mixing with PbI₂. However, both shifts are smaller than those of the NH₃⁺ peaks in the spectra of Gly-I and Gly-I+PbI₂ films from 3029 to 3108 cm^{−1}.^[31] The FTIR results indicate that Gly-I has the strongest interaction with perovskite.^[7,32,33] As a supplement to the FTIR data, high-resolution X-ray photoelectron spectroscopy (XPS) was conducted to further confirm the bonding relationship between Gly-X and PbI₂. As presented in the high-resolution Pb 4f XPS spectra (Figure 2d–f), two main peaks of Pb 4f_{5/2} and Pb 4f_{7/2} are apparent in all of the films. The Pb 4f peaks of the control film without additive lie at 143.52 and 138.64 eV, respectively, while the films with Gly-Cl, Gly-Br and Gly-I additives show the peaks at 143.47 and 138.58 eV, 143.38 and 138.53 eV, and 143.20 and 138.28 eV, respectively. All these peaks from Pb 4f shifted to lower binding energies, indicating that there is an interaction between the Gly-X and PbI₂. Meanwhile, the peaks from N 1s shifted to higher binding energies in the PbI₂ films with Gly-X, as shown in Figure 2g–i. Both the Pb 4f and N 1s shifts of the PbI₂ film with Gly-I are the largest, indicating the strongest interaction between Gly-I and PbI₂, which agrees with the results from FTIR measurement. Moreover, as shown in Figure 2j–l, the ¹H NMR spectra for the O–H bonds of Gly-X showed upfield shifts after the addition of PbI₂, which

proves the formation of O–H⋯I hydrogen bonding between Gly-X and PbI₂.^[34] Obviously, the ¹H NMR spectrum for the O–H of Gly-I has the largest shift, indicating the strongest hydrogen bonding interaction with I of PbI₂. The weak shifts of the ¹H NMR spectra for the O–H bonds of Gly-Cl and Gly-Br could be due to the preferential interaction between O–H and Cl/Br.

To entirely evaluate the impact of Gly-X additives on the photovoltaic performance of CsPbI₂Br PSCs, an n-i-p device with the planar structure glass/FTO/TiO₂/CsPbI₂Br(Gly-X)/Spiro-OMeTAD/Au was fabricated. As presented in Figure 3c, we compared the photovoltaic performance of the devices incorporated with either Gly-Cl, Gly-Br, or Gly-I. The measured photovoltaic parameters are summarized in Table 1, where distinct improvements were observed in the open-circuit voltage (V_{OC}) and fill factor (FF) with the incorporation of Gly-X. The device with Gly-I delivers a champion power conversion efficiency (PCE) as high as 17.26% and achieved a high V_{OC} of 1.33 V, short-circuit current density (J_{SC}) of 16.04 mA cm^{−2} and FF of 80.92%. Meanwhile, the best control device shows an inferior PCE of 15.87%, with V_{OC} of 1.30 V, J_{SC} of 15.85 mA cm^{−2} and FF of 76.80%. As presented in Figure S14 and Tables S3 in Supporting Information, the dependence of the device performance on the concentration of the Gly-I additive was also investigated. The optimized concentration of Gly-I is 6%. The valence band alignment between the perovskite and hole transport layer (HTL) is vital for efficient hole extraction and transport. Ultraviolet photoelectron spectroscopy (UPS) was conducted to study the influence of Gly-X additives on the energy band alignment of the perovskite film (Figures S15 and S16, Supporting Information). The schematic energy-band alignment of the CsPbI₂Br PSCs with Gly-X additives is shown in Figure 3b. The valence band maximum (VBM) of the control film is −5.86 eV, which is 0.64 eV lower than the highest occupied molecular orbit (HOMO) of the HTL (−5.22 eV).^[35] Meanwhile, the VBM positions of the films with Gly-Cl, Gly-Br, and Gly-I additives are located at −5.82, −5.84, and −5.63, respectively. All the VBM positions are shifted upward, which ensures better energy-level matching. The VBM of the CsPbI₂Br film with Gly-I was shifted up to −5.63 eV. Therefore, the energy difference between the VBM of the perovskite film and the HOMO of the HTL is reduced to only 0.41 eV, which is conducive to reducing the energy loss and favorable for photogenerated hole extraction from the perovskite to the Spiro-OMeTAD. External quantum efficiency (EQE) spectra of devices w/o Gly-I are shown in Figure 3d. The photoelectron collection in the wavelength range of 360–650 nm was clearly enhanced by the additive. The integrated current density values of the control and Gly-I-added devices are 15.55 and 15.87 mA cm^{−2}, respectively, which coincide with the values derived from the J–V curves in Figure 3c. The improved EQE can be attributed to the improved quality of the perovskite film. Figure 3e shows the steady-state current density and PCE of the PSCs, which are obtained by tracking the current density at the (initial) maximum-power-point (MPP) voltage. A stabilized PCE of 17.21% is obtained for the PSC with Gly-I at the maximum power point (1.10 V), which is in good agreement with the PCE achieved from the J–V measurement. The statistical photovoltaic parameter distributions of 50 independent cells (each) without and with Gly-I are

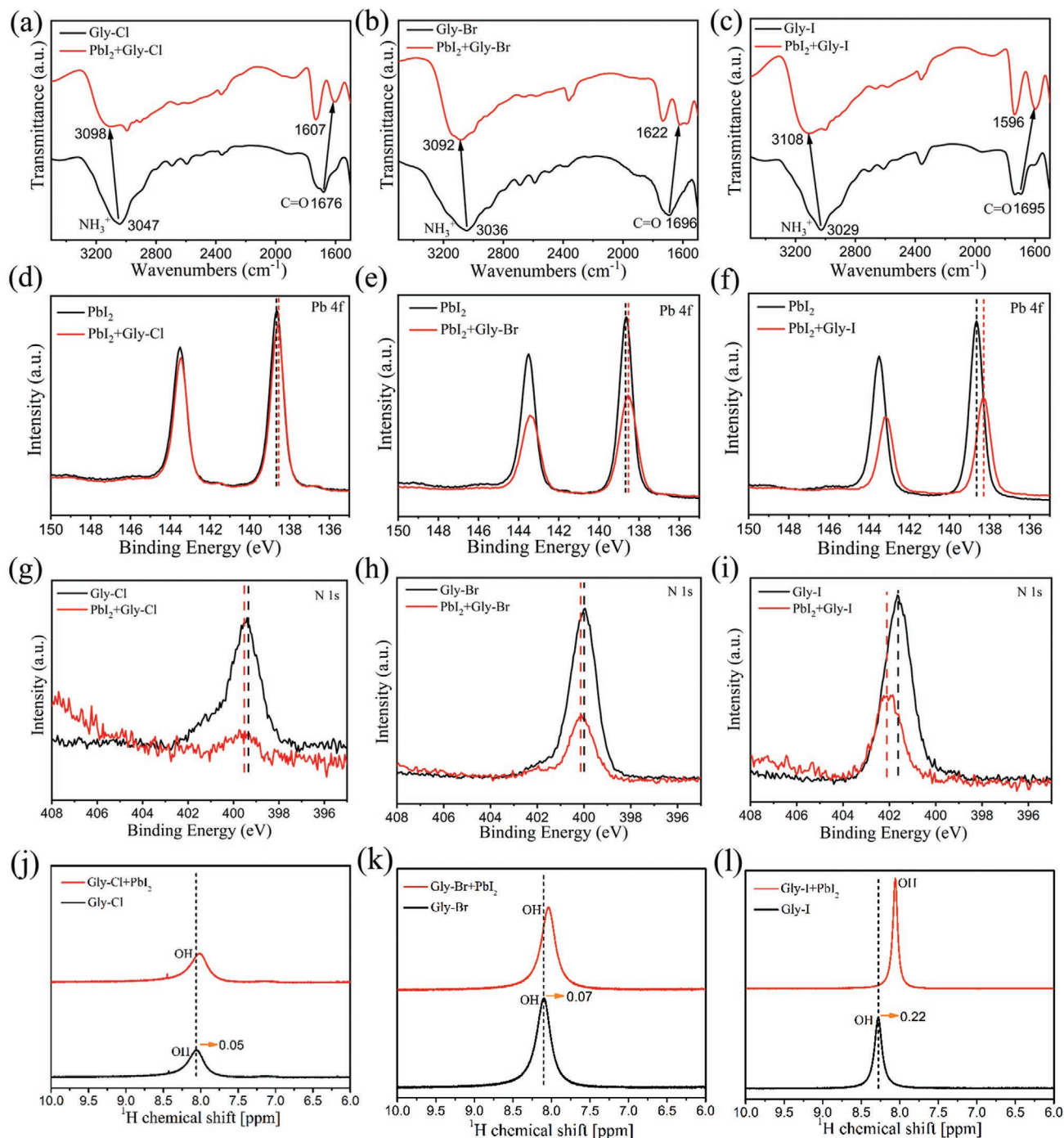


Figure 2. a–c) FTIR spectra of Gly-X solutions w/wo PbI_2 additive. d–f) Pb 4f XPS spectra of PbI_2 films w/wo Gly-X additive. g–i) N 1s spectra of Gly-X films w/wo PbI_2 additive. j–l) ^1H NMR spectra of Gly-X solutions w/wo PbI_2 additive.

shown in Figure 3f and Figure S17 in Supporting Information. Compared with the control device, all the photovoltaic parameters of device with Gly-I additive present higher values with narrow distributions, and the improved PCE stems mainly from improved V_{OC} and FF. These results permit the conclusion that Gly-I additive can undoubtedly boost the photovoltaic performance of the PSCs.

To quantitatively evaluate the effect of Gly-I additive on the trap density of perovskite films, space-charge limited current (SCLC) characterization was undertaken on an electron-dominated device (FTO/ TiO_2 /perovskite/PCBM/Ag). As illustrated in Figure 3g, it is clear that the trap-filled limit voltage (V_{TFL}) is reduced by the addition of Gly-I, from 0.54 V for the control film to 0.22 V for the perovskite with Gly-I additive. According

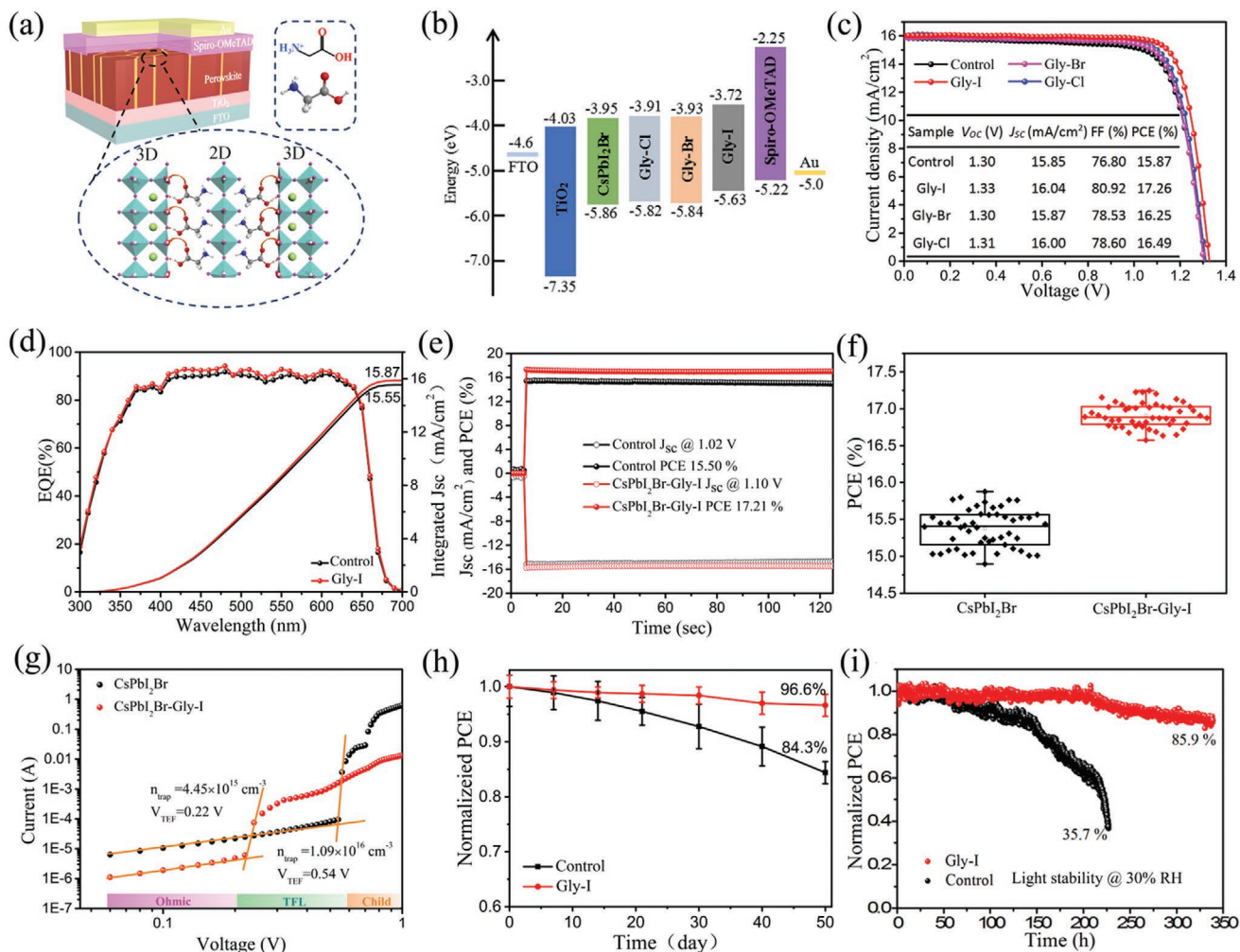


Figure 3. a) Schematic image of a CsPbI₂Br PSC with the structure FTO/TiO₂/CsPbI₂Br(Gly-I)/Spiro-OMeTAD/Au. b) Energy-level alignment and c) J-V curves of the CsPbI₂Br PSCs with Gly-X additives. d) EQE spectra, e) Stable output curves, f) Box charts of PCE, and g) Space-charge-limited current versus voltage for the FTO/TiO₂/CsPbI₂Br/PCBM/Ag and FTO/TiO₂/CsPbI₂Br(Gly-I)/PCBM/Ag devices. h) The air stability and i) light stability (T: 30 °C, RH: ≈30% in air) of the CsPbI₂Br PSCs w/o Gly-I additive.

to the equation $N_{\text{trap}} = (2\epsilon\epsilon_0 V_{\text{TFL}})/(eL^2)$, the corresponding trap densities for the control and optimized perovskite films are calculated as 1.09×10^{16} and $4.45 \times 10^{15} \text{ cm}^{-3}$, respectively. The reduced trap density induced by the Gly-I additive is attributed to the effective passivation effect of 2D perovskite on the GBs of 3D perovskite film and the improvement of perovskite crystal quality, as demonstrated by the PL, TRPL, and XRD results.^[36,37]

To further study the effect of the Gly-I additive on the stability of the PSCs, the long-term storage stability was characterized

Table 1. Summary of the photovoltaic parameters of the best CsPbI₂Br PSCs without and with Gly-X.

Sample	V _{OC} [V]	J _{SC} [mA cm ⁻²]	FF [%]	PCE [%]
Control	1.30	15.85	76.80	15.87
Gly-I	1.33	16.04	80.92	17.26
Gly-Br	1.30	15.87	78.53	16.25
Gly-Cl	1.31	16.00	78.60	16.49

using unencapsulated devices stored under ambient conditions (T: ≈ 30 °C, RH: 30%). As shown in Figure 3h, the devices with Gly-I additive still retained ≈96.6% of their initial PCEs after storage for 50 days, while the control devices only retained ≈84.3% of their initial values. Furthermore, the operational stability of encapsulated devices was characterized under MPP tracking with continuous one-sun irradiation using a light-emitting diode (LED) under ambient conditions (T: ≈30 °C, RH: ≈30%). As shown in Figure 3i, for the Gly-I-treated device, 85.9% of its PCE remains after 340 h MPP tracking, while the PCE of the control device decreased to 35.7% within 227 h. Therefore, the Gly-I additive can significantly improve the ambient and light stability of the CsPbI₂Br PSCs.

Ion migration is a critical issue that limits the stability of PSCs and cannot be prevented by encapsulation. Light-induced ion migration will lead to changes in composition and morphology, which cause phase segregation in mixed-halide perovskite. Our CsPbI₂Br film has an optical bandgap of 1.91 eV; the wider bandgap enhances its possible application in tandem

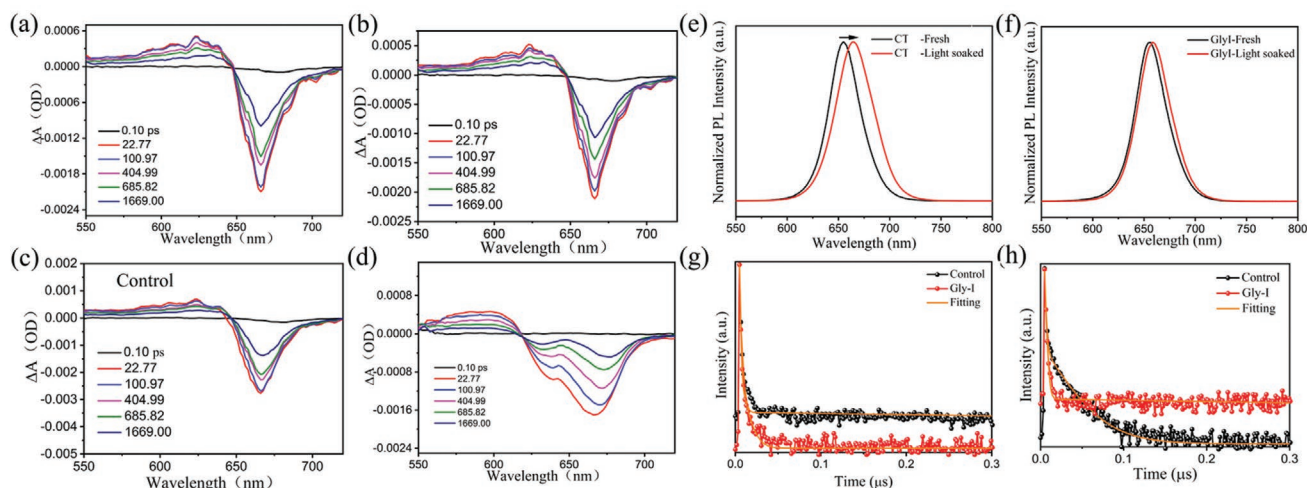


Figure 4. TA spectra at various delay times before and after light soaking, respectively, for a,b) the perovskite film with Gly-I additive and c,d) the control perovskite film. PL spectra before and after illumination for 120 min of e) pristine CsPbI₂Br film and f) CsPbI₂Br film with Gly-I additive. TRPL spectra of perovskite devices excited by a 510 nm laser from the TiO₂ side, g) before and h) after light soaking, respectively.

solar cells, but it suffers light-induced phase segregation more significantly than narrow-bandgap perovskites. The phase segregation phenomenon was observed in the TA spectra, as illustrated in Figure 4a,b. For the optimized perovskite film with Gly-I additive, the bleach peak at 660 nm remained almost unchanged after continuous illumination for 120 min. In contrast, the control perovskite film showed a decreased bleach peak at 660 nm, accompanied by a new bleach peak at 635 nm (Figure 4c,d), which is in accord with phase segregation and formation of the bromide-rich phase. Therefore, the 2D perovskite around the GBs of the 3D perovskite domains can improve the phase stability by suppressing halide ion migration. To further explore the influence of the 2D perovskite on the photostability of the 3D perovskite film, PL measurements were conducted on fresh films and perovskite films illuminated for 120 min. As shown in Figure 4e,f, the control perovskite exhibited a red-shifted PL peak with broadened full-width at half-maximum (FWHM) after illumination for 120 min, demonstrating poor photostability.^[38–40] The obvious red-shift and widening of the PL peak can be attributed to the deteriorated quality of the perovskite film with many defects caused by phase separation. By contrast, a small change was observed in the 2D/3D hybrid perovskite, confirming the significantly suppressed phase segregation.

To further understand the influence of the 2D perovskite on the photostability of inorganic PSCs, TRPL was conducted on PSCs before and after 120 min illumination at open-circuit conditions under excitation by a laser with 510 nm wavelength. As shown in Figure 4g,h, the light-soaked control PSC presents a longer TRPL decay lifetime than the fresh device, demonstrating less-efficient carrier transport to the electrodes in the soaked device.^[41] The incident laser from the TiO₂ side generates excessive carriers mainly in the perovskite near the perovskite/TiO₂ interface. Most of the photogenerated electrons should be quickly extracted to the TiO₂, and the corresponding TRPL decay reflects the transport of photogenerated holes from the perovskite to Spiro-OMeTAD. This result indicates that the transport of holes was impeded after light soaking in the

control device. In contrast, the devices with the 2D/3D configuration maintained fast extraction of holes after light soaking, as illustrated in Figure 4h.

According to all the above analysis, the function of Gly-I is summarized in Figure S18, Supporting Information. During the crystallization process, Gly-I can interact with PbI₂/PbBr₂ to retard the fast reaction between PbI₂/PbBr₂ and CsI, inducing a well-aligned CsPbI₂Br film with preferential orientation. After crystallization, the C=O and –OH groups in the organic cation of the 2D Gly₂PbI₄ perovskite formed at the GBs of 3D domains can interact with Pb²⁺ and I[–] ions of the 3D perovskite through covalent and hydrogen bonding, respectively. These interactions can simultaneously afford a passivation effect to inhibit charge trapping and recombination, a protection effect as a barrier to moisture invasion from the GBs, and a hindrance effect to block iodine migration and thereby suppress phase separation. More important, the strong interaction between 2D and 3D perovskite can also stiffen the corner-sharing [PbX₆]^{4–} octahedron network to stabilize the α -phase CsPbI₂Br.^[42,43] All together, the Gly-I additive plays multiple roles in regulating the crystallization process, passivating defect states, and stabilizing the phase structure of the CsPbI₂Br perovskite.

To further confirm the above experimental conclusions, first-principles density function theory (DFT) calculations were performed to investigate the interaction energies between Gly-X and PbI₂/perovskite and the influence of Gly-X on the formation energy of iodide vacancies (V_I) and the iodine migration energy in the CsPbI₂Br film. The calculated structures for Gly-X with PbI₂ are presented in Figure S19, Supporting Information. The binding energy of Gly-I with PbI₂ is 1.628 eV, which is higher than those of Gly-Cl with PbI₂ (1.537 eV) and Gly-Br with PbI₂ (1.446 eV), as is consistent with the FTIR and XPS results. To reduce the amount of calculation, a 2 × 2 × 3 supercell of CsPbI₃ was employed to calculate the binding energy of Gly-X with CsPbI₃ perovskite, the formation energy of V_I and migration energy of iodine. (The calculation details are given in the experimental section). As illustrated in Figure 5a, Gly-I has the highest binding energy to CsPbI₃ perovskite (1.627 eV) in

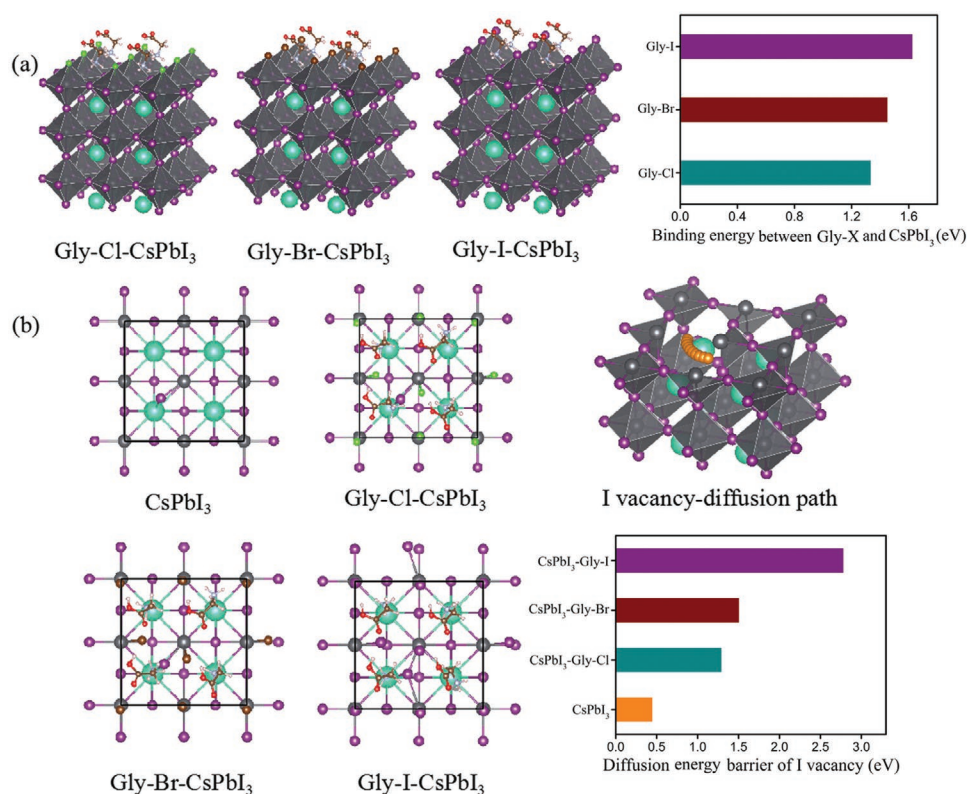


Figure 5. a) DFT calculation models and the calculated binding energy between Gly-X and CsPbI₃ b) DFT calculation models, V_I diffusion path and diffusion barrier energy of V_I in CsPbI₃ and Gly-X-treated CsPbI₃.

comparison with Gly-Br (1.452 eV) and Gly-Cl (1.335 eV). Meanwhile, the calculations show the formation of V_I in CsPbI₃ is energetically less favorable after Gly-X treatment (Figure S20, Supporting Information), which is conducive to reducing the number of vacancy sites for ion migration. Furthermore, the ionic migration energy of CsPbI₃ perovskite is increased significantly after Gly-X treatment. As shown in Figure 5b, the migration energy barrier of V_I in CsPbI₃ is only 0.449 eV; in contrast, Gly-I-treated CsPbI₃ presents a much higher value of 2.783 eV, indicating that the migration process will be significantly inhibited in the Gly-I-treated CsPbI₃.^[44,45] The calculated results are consistent with the results of TA and PL (Figure 4) as well as the stability performance of control and Gly-I-treated CsPbI₂Br solar cells. Thus, Gly-I treatment should provide a promising opportunity for highly stable CsPbI₂Br devices because it would effectively suppress the ion migration-induced decomposition of perovskite, degradation of charge transport layers, and corrosion of metal electrodes.

3. Conclusion

Gly-X additives were developed as passivating agents to improve the performance of CsPbI₂Br solar cells. Gly-X can not only modulate the crystallization process of the CsPbI₂Br perovskite to increase crystal quality but also generate 2D Gly₂PbI₄ perovskite along the GBs of the 3D CsPbI₂Br perovskite to block the migration of halide ions and enhance the photostability of the

perovskite. As a result, 2D Gly₂PbI₄ perovskite suppresses phase separation and significantly improves the long-term operational stability of the photovoltaic devices. The champion device based on the 2D/3D hybrid configuration exhibited a high PCE of 17.26% with a high V_{OC} of 1.33 V and excellent stability. An unencapsulated device retained 96.6% of its initial efficiency after 50 days storage in ambient air, and the efficiency of encapsulated device decreased only by 14.1% after 340 h continuous illumination (AM 1.5) under ambient conditions, representing one of the most stable mixed-halide inorganic PSCs reported so far.

4. Experimental Section

Materials: Cesium iodide (CsI, 99.99%), lead bromide (PbBr₂, 99.99%), lead iodide (PbI₂, 99.99%), and lead acetate (PbAc₂, 99.5%), were purchased from Xi'an Polymer Light Technology Corp. PbI₂(DMSO) and PbBr₂(DMSO) were prepared by the antisolvent method.^[46] The glycine, hydroiodic acid, hydrobromic acid, and hydrochloric acid were purchased from Alfa Aesar. N,N-dimethylformamide (DMF) and dimethylsulfoxide (DMSO) were purchased from Shanghai Aladdin Biochemical Technology Co., Ltd.

Synthesis of Gly-X (X = Cl, Br, and I): Glycine (Gly) and HX (I, Br, and Cl) were mixed with a 1:1 molar ratio, and 5 mL ethanol was added into the solution. The solvent was removed using a rotary evaporator at 70 °C under vacuum to obtain a solid powder of Gly-X. The powder was then purified by washing with diethyl ether several times, followed by drying at 60 °C for 24 h in a vacuum oven to obtain the final product.

Device Fabrication: FTO glass substrates were sequentially cleaned with ethanol, acetone, and isopropanol in an ultrasonic bath for 30 min

and then dried with N₂. The cleaned FTO glass substrates were then treated with UV-Ozone for 10 min prior to the deposition of TiO₂. The TiO₂ layer was deposited by immersing FTO glass substrates in 200 mL aqueous solution with 4.5 mL titanium tetrachloride for 60 min at 70 °C, then rinsed with distilled water and annealed at 200 °C for 30 min. The CsPbI₂Br precursor solution was prepared by dissolving PbBr₂(DMSO), PbI₂(DMSO), CsI and PbAc₂ (molar ratio = 1:1:2:0.023) in DMF and DMSO (17:3 v/v). For the perovskite with Gly-X additive, Gly-X was added at 1%, 3%, 6%, and 9% molar ratio to the perovskite solution. The perovskite precursor solution with and without Gly-X was spin-coated at 1000 rpm for 10 s, followed by 4000 rpm for 40 s. Afterward, the film was annealed at 35 °C for 6 min, 120 °C for 10 min, and 180 °C for 4 min to obtain the perovskite layer. The hole-transport layer was prepared by spin-coating Spiro-OMeTAD solution (90 mg mL⁻¹) doped with 36 μ L t-BP and 22 μ L Li-TFSI (520 mg mL⁻¹) solution in acetonitrile at 5000 rpm for 30 s onto CsPbI₂Br films to produce a TiO₂/perovskite/Spiro-OMeTAD architecture. Finally, an 80 nm Au electrode was deposited by thermal evaporation through a shadow mask to form a device with an active area of 0.09 cm².

Density Functional Theory (DFT) Calculation: The calculation was performed using VASP code in the framework of the PBE approximation. The van der Waals interaction was treated by the Tkatchenko-Scheffler method. The energies of glycine hydrohalide molecules and interaction energies between glycine hydrohalide molecules and PbI₂ were calculated in a volume of 20 \times 20 \times 20 Å³. The k-mesh was set to 1 \times 1 \times 1. The lattice constant of CsPbI₃ perovskite was set to 6.16 Å, which was obtained by optimizing a cubic CsPbI₃ unit cell. The glycine hydrohalides were modeled to be distributed on the CsPbI₃ (001) surface. The binding energy of a single glycine hydrohalide molecule with CsPbI₃ was obtained by comparing the energies of a CsPbI₃ slab (2 \times 2 \times 3 unit cells in the supercell) and a glycine hydrohalide covered CsPbI₃ slab. The defect formation energy of the I vacancy was obtained by comparing the energies of a glycine hydrohalide-covered CsPbI₃ slab and a similar slab with one I vacancy on the surface of the CsPbI₃ layer. The dimension of the calculation was set to 12.32 \times 12.32 \times 50 Å³. The k-mesh was set to 5 \times 5 \times 1. The nudged elastic band method was employed to obtain the diffusion barrier of the I vacancy on the perovskite surface. A supercell composed of 2 \times 2 \times 2 unit cells was used to construct the CsPbI₃ slab. The dimension of the calculation was set to 12.32 \times 12.32 \times 50 Å³. The k-mesh was set to 3 \times 3 \times 1 to save calculation resources. In all the calculations, the cut-off energy was set to 500 eV and the convergence condition was set to 10⁻⁵ eV.

Characterization: XRD patterns of the perovskite films were acquired on a D/MAX 2400 diffractometer. The absorption spectra of perovskite films were measured using a UV-vis NIR spectrophotometer (PerkinElmer, Lambda 950). PL (excitation at 510 nm) spectra were measured using a FLS980 spectrometer (Edinburgh Instruments Ltd), and TRPL spectra were measured with a PicoQuant FluorQuanta 300. The SEM images of perovskite films were obtained by field-emission scanning electron microscopy (SEM, Hitachi, SU-8020). XPS and UPS of the perovskite films were carried out using a photoelectron spectrometer (ESCALAB250Xi, Thermo Fisher Scientific). FTIR spectra were obtained with a Bruker Vertex 70. The TEM images were acquired by field-emission TEM (G2 F20). The J-V curves of the inorganic PSCs were measured using a Keithley 2400 SourceMeter under AM 1.5G illumination at 100 mW cm⁻². The external quantum efficiencies (EQEs) of the PSCs were recorded using a QTest Station 2000ADI system (CrownTech Inc.). EIS analysis was performed on a Zahner Electrochemical Workstation. Water contact angles were measured using a DataPhysics OCA 20.

Statistics Analysis: All statistical analysis were performed with Origin Pro 9. All the data keep two significant digits after the decimal points by the rounding-off method. The data obtained from SEM, XRD, UV-vis, PL, TA, TEM, XPS, FT-IR, NMR, UPS, DFT, J-V, EQE, and I-T are the original data without normalized. Bi-exponential decay function was applied to TRPL decays to infer the carrier extraction/recombination. The other data was obtained by transferring corresponding original data according to the calculation formula. Linear fittings were applied to

SCLC (Figure 3g). The statistical distribution data of PCE, J_{sc}, Voc, and FF were got from 50 devices each.

Supporting Information

Supporting Information is available from the Wiley Online Library or from the author.

Acknowledgements

J.X. and J.C. contributed equally to this work. The authors acknowledge support from the National Natural Science Foundation of China (62074095), the Fundamental Research Funds for the Central Universities (GK202002001), the 111 Project (Grant No. B21005), and the DNL Cooperation Fund CAS (DNL180311).

Conflict of Interest

The authors declare no conflict of interest.

Data Availability Statement

Research data are not shared.

Keywords

2D, CsPbI₂Br, grain boundaries, high efficiency, phase stability, suppress ion migration

Received: March 11, 2022

Revised: May 10, 2022

Published online:

- [1] R. J. Sutton, G. E. Eperon, L. Miranda, E. S. Parrott, B. A. Kamino, J. B. Patel, M. T. Hörantner, M. B. Johnston, A. A. Haghighirad, D. T. Moore, H. J. Snaith, *Adv. Energy Mater.* **2016**, *6*, 1502458.
- [2] M. A. Becker, R. Vaxenburg, G. Nedelcu, P. C. Sercel, A. Shabaev, M. J. Mehl, J. G. Michopoulos, S. G. Lambrakos, N. Bernstein, J. L. Lyons, T. Stoferle, R. F. Mahrt, M. V. Kovalenko, D. J. Norris, G. Raino, A. L. Efros, *Nature* **2018**, *553*, 189.
- [3] L. Yan, Q. Xue, M. Liu, Z. Zhu, J. Tian, Z. Li, Z. Chen, Z. Chen, H. Yan, H. L. Yip, Y. Cao, *Adv. Mater.* **2018**, *30*, 1802509.
- [4] H. Min, D. Y. Lee, J. Kim, G. Kim, K. S. Lee, J. Kim, M. J. Paik, Y. K. Kim, K. S. Kim, M. G. Kim, T. J. Shin, S. Il Seok, *Nature* **2021**, *598*, 444.
- [5] C. Eames, J. M. Frost, P. R. Barnes, B. C. O'Regan, A. Walsh, M. S. Islam, *Nat. Commun.* **2015**, *6*, 7497.
- [6] J. He, J. Su, Z. Lin, J. Ma, L. Zhou, S. Zhang, S. Liu, J. Chang, Y. Hao, *Adv. Sci.* **2021**, *8*, 2101367.
- [7] Y. Zhao, P. Zhu, S. Huang, S. Tan, M. Wang, R. Wang, J. Xue, T. H. Han, S. J. Lee, A. Zhang, T. Huang, P. Cheng, D. Meng, J. W. Lee, J. Marian, J. Zhu, Y. Yang, *J. Am. Chem. Soc.* **2020**, *142*, 20071.
- [8] W. Q. Wu, P. N. Rudd, Q. Wang, Z. Yang, J. Huang, *Adv. Mater.* **2020**, *32*, 2000995.
- [9] J. Cao, S. X. Tao, P. A. Bobbert, C. P. Wong, N. Zhao, *Adv. Mater.* **2018**, *30*, 1707350.

- [10] T. He, Y. Jiang, X. Xing, M. Yuan, *Adv. Mater.* **2020**, 32, 1903937.
- [11] X. Fu, T. He, S. Zhang, X. Lei, Y. Jiang, D. Wang, P. Sun, D. Zhao, H.-Y. Hsu, X. Li, M. Wang, M. Yuan, *Chem.* **2021**, 7, 3131.
- [12] T. Liu, J. Zhang, M. Qin, X. Wu, F. Li, X. Lu, Z. Zhu, A. K. Y. Jen, *Adv. Funct. Mater.* **2021**, 31, 2009515.
- [13] J. Kim, A. J. Yun, B. Gil, Y. Lee, B. Park, *Adv. Funct. Mater.* **2019**, 29, 1905190.
- [14] M. M. Tavakoli, W. Tress, J. V. Milić, D. Kubicki, L. Emsley, M. Grätzel, *Energy Environ. Sci.* **2018**, 11, 3310.
- [15] J. Zhuang, Y. Wei, Y. Luan, N. Chen, P. Mao, S. Cao, J. Wang, *Nanoscale* **2019**, 11, 14553.
- [16] J. Wang, J. Zhang, Y. Zhou, H. Liu, Q. Xue, X. Li, C. C. Chueh, H. L. Yip, Z. Zhu, A. K. Y. Jen, *Nat. Commun.* **2020**, 11, 177.
- [17] J. He, J. Liu, Y. Hou, Y. Wang, S. Yang, H. G. Yang, *Nat. Commun.* **2020**, 11, 4237.
- [18] Y. Han, H. Zhao, C. Duan, S. Yang, Z. Yang, Z. Liu, S. Liu, *Adv. Funct. Mater.* **2020**, 30, 1909972.
- [19] H. Zhao, Y. Han, Z. Xu, C. Duan, S. Yang, S. Yuan, Z. Yang, Z. Liu, S. Liu, *Adv. Energy Mater.* **2019**, 9, 1902279.
- [20] D. Lin, T. Zhang, J. Wang, M. Long, F. Xie, J. Chen, B. Wu, T. Shi, K. Yan, W. Xie, P. Liu, J. Xu, *Nano Energy* **2019**, 59, 619.
- [21] Y. Lv, X. Song, Y. Yin, Y. Feng, H. Ma, C. Hao, S. Jin, Y. Shi, *ACS Appl. Mater. Interfaces* **2020**, 12, 698.
- [22] P. Chen, Y. Bai, S. Wang, M. Lyu, J. H. Yun, L. Wang, *Adv. Funct. Mater.* **2018**, 28, 1706923.
- [23] G. Grancini, C. Roldan-Carmona, I. Zimmermann, E. Mosconi, X. Lee, D. Martineau, S. Narbey, F. Oswald, F. De Angelis, M. Graetzel, M. K. Nazeeruddin, *Nat. Commun.* **2017**, 8, 15684.
- [24] A. A. Sultano, P. Caprioglio, N. Drigo, Y. J. Hofstetter, I. Garcia-Benito, V. I. E. Quelo, D. Neher, M. K. Nazeeruddin, M. Stollerfoht, Y. Vaynzof, G. Grancini, *Chemistry* **2021**, 7, 1903.
- [25] X. Liu, X. Wang, T. Zhang, Y. Miao, Z. Qin, Y. Chen, Y. Zhao, *Angew. Chem., Int. Ed.* **2021**, 60, 12351.
- [26] T. Kong, H. Xie, Y. Zhang, J. Song, Y. Li, E. L. Lim, A. Hagfeldt, D. Bi, *Adv. Energy Mater.* **2021**, 11, 2101018.
- [27] P. Li, Y. Zhang, C. Liang, G. Xing, X. Liu, F. Li, X. Liu, X. Hu, G. Shao, Y. Song, *Adv. Mater.* **2018**, 30, 1805323.
- [28] Y. Cai, J. Wen, Z. Liu, F. Qian, C. Duan, K. He, W. Zhao, S. Zhan, S. Yang, J. Cui, S. Liu, *J. Energy Chem.* **2022**, 65, 480.
- [29] Z. Wang, Q. Wei, X. Liu, L. Liu, X. Tang, J. Guo, S. Ren, G. Xing, D. Zhao, Y. Zheng, *Adv. Funct. Mater.* **2020**, 31, 2008404.
- [30] M. Liu, Y. Chen, C. S. Tan, R. Quintero-Bermudez, A. H. Proppe, R. Munir, H. Tan, O. Voznyy, B. Scheffel, G. Walters, A. P. T. Kam, B. Sun, M. J. Choi, S. Hoogland, A. Amassian, S. O. Kelley, F. P. G. de Arquer, E. H. Sargent, *Nature* **2019**, 570, 96.
- [31] S. Tan, J. Shi, B. Yu, W. Zhao, Y. Li, Y. Li, H. Wu, Y. Luo, D. Li, Q. Meng, *Adv. Funct. Mater.* **2021**, 31, 2010813.
- [32] R. Wang, K. Wang, Z. Wang, Y. Luo, D. Fenning, G. Xu, S. Nuryyeva, T. Huang, Y. Zhao, J. L. Yang, J. Zhu, M. Wang, S. Tan, I. Yavuz, K. N. Houk, Y. Yang, *Science* **2019**, 366, 1509.
- [33] Y. Cai, J. Cui, M. Chen, M. Zhang, Y. Han, F. Qian, H. Zhao, S. Yang, Z. Yang, H. Bian, T. Wang, K. Guo, M. Cai, S. Dai, Z. Liu, S. Liu, *Adv. Funct. Mater.* **2020**, 31, 2005776.
- [34] X. Li, M. I. Dar, C. Yi, J. Luo, M. Tschumi, S. M. Zakeeruddin, M. K. Nazeeruddin, H. Han, M. Gratzel, *Nat. Chem.* **2015**, 7, 703.
- [35] S. Yang, W. Liu, Y. Han, Z. Liu, W. Zhao, C. Duan, Y. Che, H. Gu, Y. Li, S. Liu, *Adv. Energy Mater.* **2020**, 10, 2002882.
- [36] S. Yuan, F. Qian, S. Yang, Y. Cai, Q. Wang, J. Sun, Z. Liu, S. Liu, *Adv. Funct. Mater.* **2019**, 29, 1807850.
- [37] W. Zhao, J. Xu, K. He, Y. Cai, Y. Han, S. Yang, S. Zhan, D. Wang, Z. Liu, S. Liu, *Nano Micro Lett.* **2021**, 13, 169.
- [38] K. Ma, H. R. Atapattu, Q. Zhao, Y. Gao, B. P. Finkenauer, K. Wang, K. Chen, S. M. Park, A. H. Coffey, C. Zhu, L. Huang, K. R. Graham, J. Mei, L. Dou, *Adv. Mater.* **2021**, 33, 2100791.
- [39] J. Liang, C. Chen, X. Hu, M. Xiao, C. Wang, F. Yao, J. Li, H. Wang, J. He, B. Da, Z. Ding, W. Ke, C. Tao, G. Fang, *Sol. RRL* **2021**, 5, 2100249.
- [40] H. Yu, H. Wang, T. Zhang, C. Yi, G. Zheng, C. Yin, M. Karlsson, J. Qin, J. Wang, X. K. Liu, F. Gao, *J. Phys. Chem. Lett.* **2021**, 12, 6041.
- [41] Y. Deng, S. Xu, S. Chen, X. Xiao, J. Zhao, J. Huang, *Nat. Energy* **2021**, 6, 633.
- [42] J. He, W.-H. Fang, R. Long, O. V. Prezhdo, *ACS Energy Lett.* **2018**, 3, 2070.
- [43] H. Li, X. Hao, B. Chang, Z. Li, L. Wang, L. Pan, X. Chen, L. Yin, *ACS Appl. Mater. Interfaces* **2021**, 13, 40489.
- [44] J. Chen, D. Lee, N. G. Park, *ACS Appl. Mater. Interfaces* **2017**, 9, 36338.
- [45] J.-W. Lee, S.-G. Kim, J.-M. Yang, Y. Yang, N.-G. Park, *APL Mater.* **2019**, 7, 041111.
- [46] G. Yin, H. Zhao, H. Jiang, S. Yuan, T. Niu, K. Zhao, Z. Liu, S. F. Liu, *Adv. Funct. Mater.* **2018**, 28, 1803269.